Quantifying the diffusion kinetics and spatial distributions of radiogenic ^{4}He in minerals containing proton-induced ^{3}He

David L. Shuster [a,*], Kenneth A. Farley [a], Janet M. Sisterson [b], Donald S. Burnett [a]

[a] *Division of Geological and Planetary Sciences, MC 100-23, California Institute of Technology, Pasadena, CA 91125, USA*
[b] *Northeast Proton Therapy Center, Massachusetts General Hospital, 30 Fruit St, Boston, MA, USA*

Abstract

Apatite, titanite and olivine samples were bombarded with a ~ 150 MeV proton beam to produce $\sim 10^8$ atoms/mg of spallation ^{3}He. High-precision stepped-heating experiments were then performed in which the artificial ^{3}He and, for apatite and titanite, the natural radiogenic ^{4}He were measured to characterize the diffusive behavior of each isotope. Helium-3 diffusion coefficients are in excellent agreement with concurrently and/or previously determined He diffusion coefficients for each mineral. Our results indicate that proton-induced ^{3}He is uniformly distributed and that radiation damage associated with a proton fluence of $\sim 5 \times 10^{14}$ protons/cm^2 does not cause noticeable changes in ^{4}He diffusion behavior in at least apatite and titanite. Proton-induced ^{3}He can therefore be used to establish He diffusion coefficients in minerals with insufficient natural helium for analysis or those in which the natural ^{4}He distribution is inhomogeneous. In addition, step-heating ^{4}He/^{3}He analysis of a mineral with a uniform synthetic ^{3}He concentration provides a means by which a natural ^{4}He distribution can be determined.
© 2003 Elsevier B.V. All rights reserved.

Keywords: helium; diffusion; thermochronometry; isotope; proton beam; (U–Th)/He

1. Introduction

Helium isotopes produced by radioactive decay of U and Th and by cosmic ray irradiation are useful for establishing cooling rates and exposure histories of minerals [1–3]. In a companion paper [4], we demonstrated that important information

for interpretation of such data can be obtained by stepwise heating of samples in which a uniformly distributed isotope is available. In particular, a uniform, synthetic ^{3}He distribution within minerals would be useful: (i) for studying He diffusivity in phases that do not contain sufficient natural helium for accurate measurement, and (ii) for constraining the ^{4}He concentration distribution of those that do [4]. A ^{4}He concentration distribution can be used to correct (U–Th)/He ages for diffusive helium loss in some cases, and more generally places limits on the time–temperature path experienced by a sample. Here we demonstrate

* Corresponding author. Tel.: +1-626-395-2190;
Fax: +1-626-683-0621.
E-mail addresses: dshuster@caltech.edu (D.L. Shuster),
farley@gps.caltech.edu (K.A. Farley), jsisterson@partners.org
(J.M. Sisterson), burnett@gps.caltech.edu (D.S. Burnett).

that a uniform ^{3}He distribution can be generated within minerals by bombarding them with a $\sim$150 MeV proton beam. Through stepwise heating ^{4}He/^{3}He analysis of these samples we demonstrate that accurate diffusivities and ^{4}He concentration profiles can be established using the synthetic ^{3}He.

Moderate- and high-energy proton bombardment produces spallation ^{3}He from almost all target nuclei, in exactly the same way that cosmogenic ^{3}He is produced in meteorites in space [3,5]. Spallation reactions proceed through two stages [6]. In the 'cascade' or fast stage, nucleon–nucleon scattering reactions knock out a few nucleons, leaving a residual nucleus with sufficient excitation energy to produce additional particle emission by an 'evaporation' process. As the probability of a preformed mass 3 particle in the nucleus to be scattered in the cascade stage will be small, it is likely that the dominant ^{3}He production mechanism is by evaporation. There are a large number of specific paths for the emission of ^{3}He; a probable one would be ^{40}Ca (p, pn) ^{39}Ca* $\rightarrow$ ^{36}Ar+^{3}He. Here pn refers to the cascade particles, the proton being the incident particle. The ^{39}Ca* is the excited residual which evaporates a ^{3}He. In the center of mass system of the residual nucleus, an isotropic ^{3}He distribution is generated within the solid. Most of the forward momentum of the incident proton is carried off by the cascade particles; however, there will be some forward velocity of the residual nucleus in the laboratory system, which in turn produces a slight forward peaking in the ^{3}He spatial distribution. The most probable energy of spallation ^{3}He nuclei produced by this process is $\sim$1–10 MeV [6], which translates to $\sim$1 to $\sim$50 μm stopping distances in minerals [6,7]. U series and Th series α particles have similar energies. Thus, except for the forward peaking discussed above, we expect that spallogenic ^{3}He and radiogenic ^{4}He atoms will share a common distribution of sites within the mineral, at least to the extent that U and Th are uniformly distributed. As discussed below the potential complications from the forward peaking appear to be small. For similar reasons synthetic ^{3}He should also be sited similarly to natural cosmogenic ^{3}He. Note that proton-induced ^{3}He differs significantly from neutron-activated ^{39}Ar from ^{39}K: while ^{39}Ar is derived from a specific parent isotope and resides very nearly in the original K site, ^{3}He is produced from essentially all targets and its lattice siting is not closely tied to either its parent or that of ^{4}He [4].

Proton irradiation should produce ^{3}H in subequal proportions to ^{3}He [8], and this isotope decays to ^{3}He with a half-life of 12.3 years. Although unlikely, it cannot be ruled out at present that ^{3}H might migrate and site itself differently from helium, thus complicating the use of ^{3}He as a proxy for radiogenic ^{4}He. However, because all of our experiments were performed on samples less than a few months after irradiation, the tritiogenic component can be ignored.

Spallation ^{4}He is also produced through high-energy proton bombardment, with a ^{4}He/^{3}He ratio of order 10 [5]. In most minerals of interest for (U–Th)/He chronometry the abundance of radiogenic ^{4}He will overwhelmingly dominate, such that spallation ^{4}He contributes negligibly to the ^{4}He distribution. In addition, since natural ^{3}He abundances are very low in these minerals [9], the synthetic ^{3}He is the dominant source of this isotope. Thus in a practical sense the proton technique produces essentially pure ^{3}He in minerals naturally carrying essentially pure ^{4}He.

In this work we illustrate the production of spallation ^{3}He from proton irradiation of minerals, then demonstrate how it can be used as a proxy for natural radiogenic and cosmogenic helium in step-heat diffusion experiments. Our work shows that: (i) proton irradiation does not significantly modify He diffusivities, e.g., through radiation damage; (ii) the synthetic ^{3}He distribution is sufficiently uniform for our applications; and (iii) accurate He diffusivities and concentration profiles can be obtained using proton-induced ^{3}He and the mathematical formulations presented elsewhere [4,10].

2. Methods

2.1. Proton irradiation

Our samples were bombarded with a $\sim$4.0 nA,

147 MeV proton beam generated by a synchrocyclotron at Harvard Cyclotron Laboratory over a ~ 10 h period in April, 2002. The irradiation set-up is shown in Fig. 1. The irradiations took place in air. A 12.5 mm brass aperture placed upstream of the 15 mm diameter target stack defined the diameter of the proton beam. The proton fluence was measured directly during irradiation by a thin foil transmission ionization chamber placed before the aperture. This chamber was calibrated using a Faraday cup prior to sample irradiation. The measured total fluence was 3.3×10^{14} p/cm^2; this fluence was verified by measuring the production of ^{22}Na in Al monitor foils at the front and back of the target stack. To maximize the uniformity in ^{3}He production across individual samples, a 100 μm lead scattering foil was placed upstream of the target stack to generate a broad proton beam. In this configuration the beam intensity was approximately Gaussian in shape and we estimated the beam intensity as a function of radial distance from the center of the target by measuring the proton transmission through apertures of different size.

Approximately 30 different samples ranging from ~ 1 to 50 mg each were loaded into Lucite disks; we irradiated seven disks at once (Fig. 1). Ultimately, the range of protons through the stack and the energy required for ^{3}He production
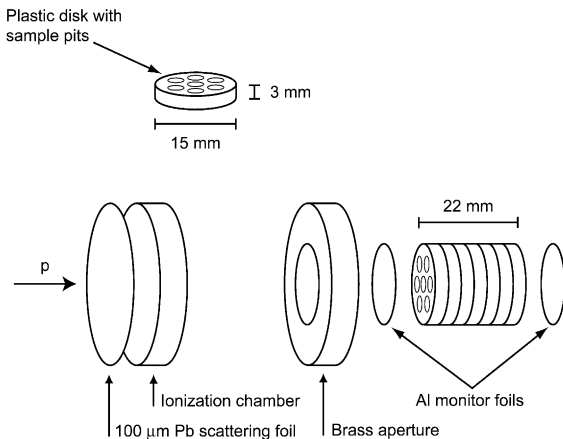

Fig. 1. Schematic showing the irradiation set-up. Samples were loaded into plastic target disks containing four or seven sample pits. Seven target disks were irradiated at once. Aluminum monitor foils were placed at the leading and leeward sides of the target stack. Note: not to scale.

limits the number of disks and thus samples that can be irradiated at once. The range of 150 MeV protons through Lucite (the bulk of our target material) is approximately ~ 13 cm, however spallation ^{3}He production drops off sharply below ~ 30 MeV [5]. This implies that ^{3}He could be induced throughout a ~ 12 cm stack.

We a priori expected potential complications for generating a uniform ^{3}He distribution. First, as discussed above, forward momentum may be transferred to the excited nucleus; a slight anisotropy in the ^{3}He ejection trajectory across a grain is expected. However, this effect appears insignificant (see Section 5). More importantly, spallogenic ^{3}He nuclei will be 'ejected' from the surfaces of the irradiated mineral just like radiogenic ^{4}He is ejected following U and Th decay [7]. Because the target minerals were loaded into Lucite disks that also produced spallogenic ^{3}He, 'ejected' ^{3}He should be approximately balanced by 'implanted' ^{3}He from neighboring target atoms. For the fine-grained samples (< 200 μm; apatite and titanite), $> 90\%$ of the grains were adjacent to other grains of exactly the same chemical composition, therefore in those cases ^{3}He ejection and implantation would be in balance. Independent experiments have confirmed this 'approximate balance' condition for other product/target combinations [11].

A final potential complication is heating of the sample during proton irradiation. Because He diffuses at moderate temperatures from many minerals, heating may cause both the natural and synthetic helium distributions to become rounded, compromising the experiment. We estimate that the proton beam energy exiting the target stack was ~ 115 MeV, depositing ~ 35 MeV within the stack. We can constrain the maximum temperature by assuming that the ~ 35 MeV is deposited within the target as kinetic energy appearing as heat. At 4.0 nA, this energy deposition translates to ~ 0.15 W, from which we estimate a maximum temperature during irradiation of ~ 1–2°C above ambient, or < 30°C. The maximum time and temperature that can be tolerated depends on the He diffusion characteristics of the mineral being investigated, but as we show below, for apatite, titanite and olivine there is no indication of diffusive rounding.

In addition to ^{3}He, proton bombardment also produces many short-lived radionuclides that could present a radiation exposure risk. Following irradiation and 5 days of decay, the samples in the target holder had an in-contact activity of $\sim$30 µSv/h (3 mrem/h), and after 10 days, $\sim$15 µSv/h. After 17 days radioactivity levels were considered sufficiently low to permit safe handling and shipment back to Caltech.

2.2. Diffusion experiments

The design of our diffusion experiments drew upon previous work in ^{40}Ar/^{39}Ar [12,13] and (U–Th)/He dating [9]. The sample was held at a known temperature (T_i) for a known time (t_i) in a volume of $\sim$300 cm^3 under static vacuum [14]. Following each heating step i, we measured released helium on a MAP 215-50 sector field mass spectrometer calibrated by external standardization. At the end of an experiment, samples were fused at $\sim$1500°C in a resistance furnace. Details of the analytical techniques are described elsewhere [1,14,15], but were modified such that both helium isotopes were detected on a pulse-counting electron multiplier. Heating steps typically yielded 1–500 cps and 10^4–10^6 cps for ^{3}He and ^{4}He, respectively. From reproducibility of standards in this response range, we estimate our measurement precision to be $\sim$5% to 0.5% relative standard error for ^{3}He (low to high count rate, respectively) and generally much better than $\sim$0.5% for ^{4}He.

We monitored and corrected for possible long-term (days) drift in sensitivity and characterized blanks by interspersing blank and standard analyses throughout an experiment. We routinely maintained diffusion cell ^{3}He blanks $<$0.2 cps ($\sim$2$\times$10^4 atoms) and ^{4}He blanks $<$1500 cps ($\sim$2$\times$10^8 atoms) during our experiments, and performed blank corrections on each measurement.

We converted measured ^{3}He step-release fractions ($F_i^{3\text{He}}$) to diffusion coefficients using [10]. From this calculation, and the temperature of each step, we generated Arrhenius plots to determine the activation energy, E_a, and frequency factor, D_o/a^2 by linear regression to define the function $D(T)/a^2 = D_o/a^2 \ \exp(-E_a/RT)$ (D is the diffusion coefficient, a is the characteristic length scale of the diffusion domain, R is the gas constant). We assumed spherical geometry and an initially uniform ^{3}He concentration profile. To verify the assumed initial condition, we incorporated temperature cycling in our experiments, i.e., we used heating schedules that included steps of both increasing (prograde) and decreasing (retrograde) temperature [4].

3. Samples

For this initial study we focused on materials with well-characterized helium diffusion parameters to test the reliability and assumptions of the method, specifically Durango apatite, titanite from the Fish Canyon tuff (FCT), and olivine from Guadalupe Island. The analyzed Durango apatite and FCT titanite were aliquots of the exact samples previously studied for ^{4}He diffusion [16,17].

The Durango apatite sample consists of fragments produced by crushing a slab cut from the interior of a large, gem-quality fluorapatite from Cerro de Mercado, Durango, Mexico [18]. ^{4}He diffusivity has been extensively studied in Durango apatite [9,16,19]. The material analyzed in this study is an aliquot of that previously analyzed by [9,16]: angular shards sieved to 160–180 µm. Some zonation of U and Th may exist within this sample [20], but its magnitude and length scale are unlikely to have affected the ^{4}He profile within individual fragments. Similarly, because the crystal interior has not experienced diffusive loss or α-ejection [7], the ^{4}He distribution is expected to be very nearly uniform.

Geochronology of the FCT was recently described [21,22]. Because the FCT titanite was collected from the quickly cooled tuff (eruption age = 28.0 $\pm$ 0.3 Ma [21]), this material is not likely to have a diffusively rounded ^{4}He distribution. The analyzed aliquot contained grains ranging from 75 to 220 µm, with 70% between 125 and 190 µm. On the average, we expect euhedral grains to have an F_T value of 0.91, representing 9% of the ^{4}He lost by α-ejection. However, most

grains were non-euhedral fragments. Despite the inherent complication of analyzing a distribution of grain sizes, the analyzed material is an aliquot of that studied for ^{4}He diffusion [17].

A gem-quality Fo_{75}–Fo_{80} olivine megacryst from Guadalupe Island [23] was also analyzed. We selected olivine free of fluid inclusions for this study, and analyzed a nearly spherical fragment of radius ~ 690 μm. Our analyses of other olivines from this locality indicate very low concentrations of natural He in this material, presumably located in fluid inclusions.

4. Results

4.1. Proton-induced ^{3}He production

Estimated proton fluences and measured ^{3}He yields are listed in Table 1. In this irradiation configuration, there was a known radial variability in the proton fluence across the disks, which we measured by determining the transmission through apertures of increasing diameter. For instance, the innermost 3.6 mm received an average fluence of $\sim 5.2 \times 10^{14}$ p/cm^2, whereas the outermost 2.8 mm received only $\sim 2.3 \times 10^{14}$ p/cm^2. Although a slight energy gradient exists along the beam axis, variability in the along-axis fluence is expected to be negligible. Diffusion experiments were performed on single or multiple (~ 200) grains from individual sample pits. Based on the apparent radial gradient, we conclude that the relative dose across a given sample pit (~ 1 mm) varied by no more than $\sim 10\%$, and we expect that individual apatite or titanite grains (~ 150

μm) received a uniform dose to within $\sim 1.5\%$. The homogeneity in ^{3}He production is supported by the ^{3}He results presented below. Because the single analyzed olivine grain diameter was approximately 1.4 mm, it could potentially have received a dose varying by $\sim 10\%$ across the grain (perpendicular to the beam direction) and any decrease in production cross section along the beam axis is negligible.

Helium-3 yields are a function of the incident proton energy, total proton fluence and target chemistry specific to a given sample, but averaged 1.9×10^8 atoms/mg. The values in Table 1 dictate the sample mass required for accurate ^{3}He detection in a step-heating experiment. For instance, we generated $\sim 10^6$ atoms of ^{3}He in a single ~ 4 μg Durango apatite shard. Given our ^{3}He sensitivity, this translates to a total response of ~ 10 cps/shard. Thus a multi-step outgassing experiment requires at least a few tens of grains and the ^{3}He measurements on apatite and titanite were performed on aggregates of ~ 200 grains (~ 1 mg mass). The olivine grain was sufficiently large that a single-grain experiment could be performed.

Based on an expected spallation ^{4}He/^{3}He production ratio of ~ 10 [5], and the observed He concentrations in the apatite [9] and titanite [17], the spallogenic ^{4}He fraction is negligible: $\sim 5 \times 10^{-4}$ and 1×10^{-4}, respectively. Spallogenic ^{4}He contributes more significantly to the ^{4}He budget of the olivine sample, amounting to perhaps 6% of the total. The natural ^{3}He abundances of the apatite and titanite samples are negligible compared to the spallation ^{3}He [9,17]. Assuming the Guadalupe olivine contains a natural ^{4}He/^{3}He

Table 1
Dose/yield summary

Phase	Fluence ($\times 10^{14}$ p/cm^2)	Proton energy (MeV)	[^{3}He] ($\times 10^8$ atoms/mg)	[^{4}He] ($\times 10^{10}$ atoms/mg)
Apatite	5.20	~ 140	1.97	367
Titanite	3.19	147	1.79	1435
Olivine	3.19	~ 140	1.82	< 3

The proton fluence of each sample was estimated by its radial position within the target stack as discussed in the text. Uncertainty in these doses is estimated to be on average $\pm 10\%$ relative error. Analytical techniques for determining ^{3}He and ^{4}He concentrations are described in [1,14,15]. We estimate the uncertainty to be better than $\pm 2\%$ for each. Note that ^{4}He in these minerals is almost exclusively natural and radiogenic rather than synthetic.
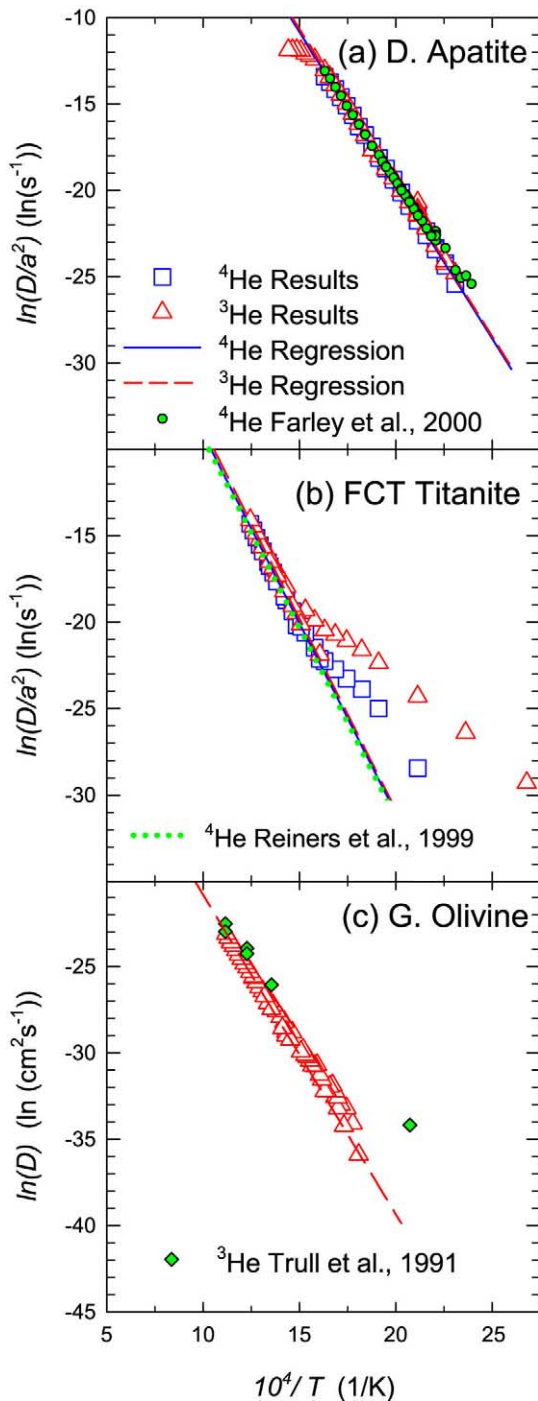
ratio of 1.4×10^5 [24], and all of the ^{4}He is natural, the natural ^{3}He content will at most be $\sim 1 \times 10^{-3}$ of the total ^{3}He budget.

4.2. Diffusion experiments

Results of the three diffusion experiments are presented as Arrhenius plots in Fig. 2a–c. The three minerals have independently known helium diffusivity with which we compare our ^{3}He results. Durango apatite and FCT titanite were previously studied in our lab for radiogenic ^{4}He diffusion [9,16,17], and we compare our olivine results with those determined using natural cosmogenic ^{3}He in a different sample by Trull et al. [25]. Regression statistics and the ^{3}He diffusion parameters D_o/a^2 and E_a are summarized for the three experiments in Table 2. We also present the concurrently determined ^{4}He results for the irradiated apatite and titanite experiments; the Guadalupe olivine sample contained insufficient ^{4}He for accurate measurement. To compare the olivine results with previous work, we converted values of $\ln(D/a^2)$ to $\ln(D)$ by dividing by the olivine grain radius, assuming that the physical grain equals the diffusion domain.

Fig. 2a presents our results for diffusion of spallogenic ^{3}He and natural ^{4}He from Durango apatite, along with previous results [16]. Because ^{4}He diffusion has been well characterized in this material [9,16] and it is known to have a uniform ^{4}He distribution, it is an ideal candidate for verifying several assumptions of our method. The ^{3}He Arrhenius plot shows strong linearity between 150 and 350°C and diffusion coefficients that are in excellent agreement with those previously determined for ^{4}He. We find within analyt-

←
Fig. 2. Arrhenius plots for (a) Durango apatite, (b) FCT titanite and (c) Guadalupe olivine. Open triangles are values calculated from ^{3}He and open squares calculated from ^{4}He for the irradiated samples. The dashed lines indicate least squares regression through subsets of the ^{3}He results and the solid lines the ^{4}He results in panels a and b. Also shown as circles in panel a are ^{4}He results from [16], as dotted line in panel b are ^{4}He results from [17], and as diamonds in panel c are cosmogenic ^{3}He results from [25] for a different olivine sample.

Table 2
Diffusion coefficient summary

Phase	Radius (μm)	Isotope	R^2	d.f.	$\ln(D_o/a^2)$ ($\ln(s^{-1})$)	($\pm$)	E_a (kJ/mol)	($\pm$)
Apatite	160–180	[3]He	0.998	22	16.03	0.32	147.87	1.32
		[4]He	0.999	22	15.82	0.20	147.65	0.85
		[4]He[a]	0.998	49	13.51	0.30	136.72	1.21
Titanite	75–220	[3]He	0.998	12	13.34	0.45	183.66	2.71
		[4]He	0.997	12	12.87	0.48	182.55	2.93
		[4]He[b]	n.a.	n.a.	12.30	0.70	182.95	10.00
Olivine	∼690	[3]He	0.999	23	3.00	0.17	153.78	1.09
		[3]He	0.993	54	0.93	0.29	139.60	1.67

Standard errors in the regression statistics are reported at the 95% confidence level. d.f., the number of degrees of freedom in the regression.
[a] From [16].
[b] From [17].

ical uncertainty equivalent diffusivity parameters for both isotopes in the irradiated experiments (Table 2).

To quantify the relationship between proton-induced [3]He and radiogenic [4]He diffusivity in Durango apatite, we present an additional experiment as a ratio evolution diagram [4] of R_{step}/R_{bulk} vs. $\sum F_i^{3\text{He}}$ (where $R = {}^4\text{He}/{}^3\text{He}$, R_{step} is the measured ratio at each step, R_{bulk} is the bulk ratio, and $\sum F_i^{3\text{He}}$ is the cumulative [3]He release fraction; Fig. 3) in which we see an effectively constant [4]He/[3]He ratio at each step of the experiment extending out to high gas yield. Deviation from the bulk ratio (R_{bulk}) occurs only during the steps at high values of $\sum F_i^{3\text{He}}$, which may indicate that [4]He diffusivity is slightly higher than [3]He (see Section 5). The results presented in Fig. 3 also indicate a lack of observable difference between the [3]He and [4]He spatial distributions.

We observe a small [3]He excess (∼1% of the total [3]He budget) in the initial steps of both Durango experiments (see Fig. 2a), where we define an excess to be a gas fraction resulting in anomalously high diffusion coefficients with respect to the main array. High diffusivity in the initial and low-temperature steps was also observed in this and previous studies of [4]He [16]. The excess may be related to small grains adhering to the shard surfaces (see Section 5). We therefore excluded these steps from Arrhenius regressions.

The resulting Durango apatite diffusion parameters are: $E_a = 148 \pm 1$ (kJ/mol) and $\ln(D_o/a^2) =$

16.0 ± 0.3 ($\ln(s^{-1})$) (S.E.M.; $n = 23$) and $E_a = 148 \pm 1$ (kJ/mol) and $\ln(D_o/a^2) = 15.8 \pm 0.2$ ($\ln(s^{-1})$) (S.E.M.; $n = 23$) for [3]He and [4]He, respectively. The [3]He and [4]He results are statistically indistin-
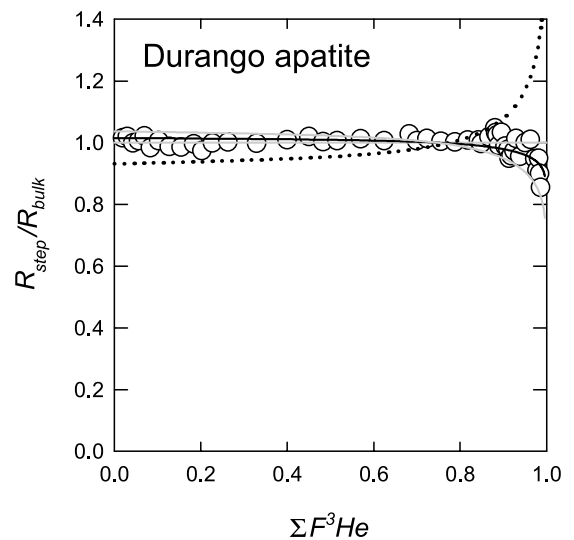

Fig. 3. Durango apatite ratio evolution diagram. Shown are measured isotope ratios for each release step, R_{step} ($R = {}^4\text{He}/{}^3\text{He}$), normalized to the bulk ratio R_{bulk} plotted vs. the cumulative [3]He release fraction, $\sum F^{3\text{He}}$. Four diffusion models are shown. The model that best fits the entire dataset, $D^{4\text{He}}/D^{3\text{He}} = 1.03$, is shown as a solid black curve with 95% confidence intervals shown as solid gray curves: $D^{4\text{He}}/D^{3\text{He}} = 1.00$ and 1.07, respectively. We also show as a dotted curve the model corresponding to the inverse root mass relationship: $D^{4\text{He}}/D^{3\text{He}} = \sqrt{m_3/m_4} = 0.868$. The size of the points roughly indicates the average analytical uncertainty throughout the experiment.

guishable from each other. The corresponding closure temperatures for each isotope are 78°C and 79°C, respectively (assuming $dT/dt = 10$°C/Myr throughout this paper). These results are in good agreement with earlier studies [16] (see comparison in Fig. 2a).

Helium-3 and ^{4}He diffusivities for FCT titanite are shown in Fig. 2b. The most obvious feature in the plot is a break in slope occurring at ~ 390°C that separates two distinct linear arrays that are present for both isotopes. A similar pattern was also observed in an unirradiated aliquot of the same material [17]. The 10 points in the lower-temperature array represent $\sim 1\%$ of the total ^{3}He budget; the ^{4}He diffusivities are consistently lower than the ^{3}He diffusivities within this array (initially by several orders of magnitude), and converge at higher ^{3}He yield (see Section 5). Reiners and Farley [17] also observed high ^{4}He diffusivity in the initial and low-temperature steps. Once the initial 1% is removed, we find good agreement between ^{3}He and ^{4}He diffusivities and a strong linear correlation between $\ln(D/a^2)$ and $10^4/T$ for steps between 350°C and 530°C, including a retrograde temperature cycle.

The regressed FCT titanite diffusion parameters from the higher-temperature array are: $E_a = 184 \pm 3$ (kJ/mol) and $\ln(D_o/a^2) = 13.3 \pm 0.5$ ($\ln(s^{-1})$) (S.E.M.; $n = 13$) and $E_a = 183 \pm 3$ (kJ/mol) and $\ln(D_o/a^2) = 12.9 \pm 0.5$ ($\ln(s^{-1})$) (S.E.M.; $n = 13$) for ^{3}He and ^{4}He, respectively. The difference between ^{3}He and ^{4}He diffusivity is statistically insignificant. The corresponding closure temperatures for each isotope are 185°C and 186°C, respectively. These results are in excellent agreement with earlier work [17] ($E_a = 176–190$ (kJ/mol) and $\ln(D_o/a^2) = 11.6–13.0$ ($\ln(s^{-1})$); $T_c = 181–201$°C for the same material. A ratio evolution diagram [4] calculated from the FCT titanite results (not shown) is consistent with a small fraction of ^{4}He lost by α-ejection or diffusion (see Section 5).

Diffusion results from the Guadalupe olivine megacryst are shown in Fig. 2c as $\ln(D)$ vs. $10^4/T$ using $a = 690$ μm. As with the apatite and titanite analyses, we observe small ^{3}He excess in the initial and low-temperature heating steps. The ^{3}He released in the initial 30 heating steps, result-

ing in anomalously high diffusivity, amounts to $\sim 1.5\%$ of the total ^{3}He budget. Once the excess is removed, we find linear correlation between $\ln(D/a^2)$ and $10^4/T$ for steps between 280 and 620°C and good agreement with ^{3}He diffusion coefficients previously determined for another olivine sample [25], particularly at higher temperatures. The results remain linear throughout a retrograde cycle between 510 and 415°C.

We present statistics for two regressions in Table 2: one including all the olivine data, the other excluding the initial steps containing excess ^{3}He. We find good agreement between the regressions with a stronger correlation coefficient for the latter ($R^2 = 0.993$ vs. $R^2 = 0.999$). The olivine diffusion parameters calculated from the regressions are $E_a = 140 \pm 2$ (kJ/mol) and $\ln(D_o/a^2) = 0.93 \pm 0.3$ ($\ln(s^{-1})$) (S.E.M.; $n = 55$) and $E_a = 154 \pm 1$ (kJ/mol) and $\ln(D_o/a^2) = 3.0 \pm 0.2$ ($\ln(s^{-1})$) (S.E.M.; $n = 24$), respectively. Although the second regression uses fewer data, we prefer it because it is based only on steps that remain linear throughout cycled heating steps. The corresponding closure temperatures for each regression are 191°C and 210°C, respectively.

5. Discussion

Our experiments show that a beam of 150 MeV protons produces sufficient spallation ^{3}He to measure in a multi-step diffusion experiment. In order to use the synthetic ^{3}He as a proxy for the diffusion of natural ^{4}He in minerals as we propose elsewhere [4] we must also establish that: (i) the ^{3}He profile is uniform across the diffusion domain; (ii) heating and/or radiation damage have not modified He release characteristics from the minerals; and (iii) ^{3}He diffuses at an equivalent rate as or a rate quantitatively relatable to ^{4}He.

5.1. ^{3}He profile uniformity

Two lines of evidence support the conclusion that the ^{3}He profile produced within individual grains by proton irradiation is essentially uniform. First, in our step-heating experiments we used a cycled heating schedule including both prograde

and retrograde steps. As we [4] and others [10] have discussed, non-uniform diffusant profiles will yield erroneous diffusion coefficients when using the standard formulation of [10], which assumes a uniform initial profile. The magnitude of this error decreases as the experiment proceeds, which causes points to deviate from linearity in an Arrhenius plot especially when retrograde steps are included [4]. The apatite experiment shown in Fig. 2a most clearly illustrates linearity on the Arrhenius plot, in both prograde and retrograde steps. With the exception of a small initial excess, which we attribute to a different phenomenon, all points lie on a single line arguing in favor of uniformity.

A second line of evidence supporting uniformity in the grains' ^{3}He spatial distribution comes from Fig. 3. For independent reasons described above we believe that the ^{4}He profile in the apatite fragments is uniform. As shown in the ratio evolution diagram (Fig. 3), the ^{4}He/^{3}He ratio is essentially invariant. Without special circumstances, this can only mean that ^{3}He and ^{4}He diffuse at approximately the same rate (see below) and that, like the ^{4}He profile, the ^{3}He profile within the individual grains is uniform. This conclusion is insensitive to any slight variability in the ^{3}He production rate that may have existed between grains (for instance grains separated by ∼1 mm during the irradiation but analyzed together). Note that these combined observations also preclude the possibility that heating during irradiation has caused diffusive rounding of the profile of either isotope. Lastly, we conclude that the slight anisotropy in ^{3}He production that we expected due to preferential forward momentum transfer to the target nucleus does not significantly bias our diffusivity results.

While the titanite and olivine both have modest deviation from both of these behaviors, it is difficult to imagine that the ^{3}He distribution is uniform in some samples but not others located just a few millimeters away.

5.2. Do ^{3}He and ^{4}He diffuse at the same rate?

The ratio evolution diagram [4] is highly sensitive to differences between ^{3}He and ^{4}He diffusivity

if each isotope has an initially uniform distribution. If ^{3}He diffusivity is higher than that of ^{4}He, we expect the measured ^{4}He/^{3}He ratios (R_{step}) to be initially lower than the bulk ratio and progressively increase to values higher than the bulk ratio as $\sum F^{^3He}$ approaches unity. Especially in the steps at high $\sum F^{^3He}$ this distillation effect can be very pronounced, yet this is not seen in the apatite data. Using a similar diagram, Trull and Kurz [26,27] found natural ^{3}He diffusivities to be 1.09, 1.04, and 1.08 times faster than ^{4}He diffusivities in olivine, clinopyroxene and basaltic glass, respectively. Each of these relationships between $D^{^3He}$ and $D^{^4He}$ deviates from the simple kinetic theory of gases which predicts $D^{^3He}/D^{^4He} = 1.15$.

From the constancy in ^{4}He/^{3}He ratio over the course of the Durango apatite experiment (Fig. 3) we conclude that proton-induced ^{3}He and radiogenic ^{4}He have nearly equivalent diffusivity in that material, with ^{4}He potentially diffusing slightly faster than ^{3}He. By calculating the residual sum of squares between our observations and various models, we find that the data are most consistent with a $D^{^4He}/D^{^3He}$ ratio of 1.03 ($^{+0.04}_{-0.03}$ at 95% confidence). If we exclude the last five data points (for $\sum F^{^3He} > 0.96$), the data are more consistent with a $D^{^4He}/D^{^3He}$ ratio of 1.00; we find a residual sum of squares that is approximately half that of the $D^{^4He}/D^{^3He} = 1.03$ model.

The kinetic theory of gases and most solid-state diffusion theories suggest a mass-dependent relationship between isotopic mass and diffusivity, but the magnitude and sign of the effect is uncertain [27] and a departure from the simple 'inverse root mass' relationship is clearly evidenced by previous work [26,27]. That we observe effectively no mass dependence of He diffusivity, or perhaps slightly higher ^{4}He diffusivity, indicates that most diffusion theories may not appropriately describe the He outgassing process in detail. For example, the process of He diffusion might be controlled by the thermally activated diffusion of lattice defects, which would have no dependence on the mass of the diffusant.

At present the conclusion that proton-induced ^{3}He and radiogenic ^{4}He diffuse at approximately the same rate has only been quantitatively estab-

lished for Durango apatite. Further experiments are required to establish the generality of this conclusion and should enable a more detailed understanding of solid-state He diffusion to be developed. It is important to recognize that the method for determining ^{4}He spatial distributions presented by Shuster and Farley [4] does not require that the diffusivities of each isotope are equivalent, so long as they are quantitatively relatable.

5.3. Effects of proton irradiation on He diffusivity

Our experiments clearly demonstrate that for the fluence we used, proton irradiation does not modify ^{4}He diffusion kinetics. This is shown by identical ^{4}He diffusivity of irradiated and unirradiated apatite and titanite. Our observations only apply to the dosage and minerals we investigated; experiments on additional minerals at higher fluences could conceivably yield different results.

Previous efforts involving nuclear irradiation followed by noble gas diffusion have underscored the need to evaluate the role of lattice damage in modifying release behavior [28–31]. Horn et al. [29] concluded that for a fast neutron fluence $< 2 \times 10^{18}$ n/cm^2, nuclear reaction-induced radiation damage to mineral lattices insignificantly affects Ar diffusion. Reactor fast neutrons produce much more lattice damage than 147 MeV protons, but even if we assume that lattice damage caused by incident protons will equivalently scale with fluence, we expect negligible damage to be associated with the irradiations in this study (2–5$\times 10^{14}$ p/cm^2). While fast neutrons lose essentially all their energy by inelastic scattering with almost every collision producing a lattice dislocation, the 147 MeV protons lose energy primarily by electronic stopping (ionizing collisions with electrons with no resulting lattice damage). About 25% of 147 MeV protons initiate nuclear spallation reactions which probably do cause lattice dislocations, but these events are spread out over many centimeters of path length. Assuming that He diffusion would be primarily affected by point defects resulting from nuclear reactions we expect radiation damage diffusion enhancements to be negligible [32].

5.4. Identifying multiple diffusion domains

The introduction of proton-induced ^{3}He enables us to identify distinct domains that are either so small or lacking retentivity that all or most of the natural ^{4}He is lost prior to analysis. The use of proton-induced ^{3}He is thus highly sensitive for 'observing' these domains. This sensitivity may account for the excess ^{3}He detected in the initial steps of the apatite and titanite experiments. For instance, we can model the observed Durango apatite ^{3}He and ^{4}He excess as being derived from 0.5 volume % of ∼0.5 µm chips adhering to the 160 µm shard surfaces. For the ^{3}He excess, the shards need not be of apatite; any material adhering to the grains, i.e., dust, plastic fragments, etc., might host spallogenic ^{3}He. The origin of this excess He is not yet completely understood but surface contamination is the leading candidate.

FCT titanite presents a more complex example. The analyzed aliquot was a mixture of grain sizes spanning 75–220 µm. We observed excess helium in the initial steps for both ^{3}He and ^{4}He (Fig. 2b), although each amounts to a negligible yet different fraction of the total (∼1% and 0.5% respectively). Assuming no ^{3}He was lost prior to analysis, and if both the ^{3}He and ^{4}He measured in these steps are predominantly derived from less retentive domains, the results are consistent with ∼50% diffusive and α-ejection ^{4}He loss from those domains. If we make a simplistic assumption that *only* two domains are present and we estimate a function $D(T)/a^2$ for the low-retention domain (by regressing a line solely through the initial 'excess' ^{3}He results), we find that the 50% discrepancy is roughly consistent with diffusive ^{4}He loss at ambient temperatures (∼20°C) over the age of the sample, ∼28 Myr.

In these examples, more careful size sorting, coupled with more careful cleaning of surfaces to eliminate adhering matter, could potentially remove the less retentive domains. When sorting is not possible, proton-induced ^{3}He may be used to quantify the mass fraction of small or low-retentivity domains that have lost ^{4}He in the geologic setting. If these domains existed in nature, this knowledge could be used to correct ages for

'missing' radiogenic ^{4}He that would have resided in those domains had they been quantitatively retentive. This approach may be important for determining absolute ages of samples having a distribution of domains such as polycrystalline materials [33].

5.5. ^{4}He profile inversion

We previously proposed a linear inversion technique to obtain ^{4}He concentration profiles from step heating of a proton-irradiated sample with a uniform ^{3}He distribution [4]. In such an experiment ^{3}He allows computation of He diffusivity, while ^{4}He release is controlled by both diffusivity and by the sought-after concentration profile. An important test of the inverse calculation is to determine the accuracy of a ^{4}He distribution derived from measurements containing analytical errors. We previously simulated such a test [4] and demonstrated the need for a regularization method (ridge regression) to filter the influence of measurement errors. Here we apply this technique to measured data.

We would like to verify the inversion result by analyzing a sample in which the initial ^{4}He profile $C_o(x)$ is known. Here we use our Durango apatite experiment for this purpose. Because the ^{4}He distribution is initially uniform in this material, we know the ^{4}He distribution at every step of the experiment [4,10]. We thus use the early steps of a stepwise outgassing experiment to diffusively evolve the initially square profile to a series of progressively more rounded profiles, then examine whether we can recover these known profiles.

Using the complete Durango apatite dataset shown in Fig. 3, we considered three cases: 0.06, 0.10 and 0.15 *deficit gas fractions* of ^{4}He removed by diffusion. We define the *deficit gas fraction* as $(N_{uniform} - N_o)/N_{uniform}$ [4]. This quantity compares the total amount of diffusant in a rounded profile (N_o) with the amount in a uniform profile ($N_{uniform}$) with concentration equivalent to that of a quantitatively retentive material. For each calculation we identified the step number at which the desired cumulative ^{4}He gas fraction ($\sum F_i^{4He}$) had been removed, then recalculated the release fractions F_i* as if that fraction had been removed

prior to the experiment. For instance, after 6% was removed, we renormalized the subsequent ^{4}He release fractions to 0.94. With the new set of F_i*, and the original set of diffusion coefficients (determined from ^{3}He), we performed the inverse calculation.

We inverted for the profiles shown using the diffusivities implied by ^{3}He release at each step, rather than from a best fit function $D(T)/a^2$ over the entire experiment, and assumed ^{3}He and ^{4}He diffusivity to be equivalent. Although $D(T)/a^2$ determined from an Arrhenius plot (e.g., Fig. 2) adequately describes He diffusion kinetics for many applications, there are several reasons why diffusivities implied by ^{3}He release at each step should be used for this computation. Only the values τ_i (where $\tau = D(T)t/a^2$, and $\tau_i = \Sigma \tau(T_i, t_i)$; see equation 3 in [4]) for each step in the outgassing experiment are actually required, so there is no need for temperature extrapolation or interpolation. Using the values at each step is preferred since they are most closely related to ^{3}He observations and are unaffected by uncertainty in the temperature T_i of each step. Additionally, the ridge regression is not designed to regularize systematic errors in the design matrix that may be introduced by using an Arrhenius regression. The design matrix relates measured remaining fractions to the initial concentration profile (see equation 5 in [4]), and incorporates two exponential functions of activation energy E_a, i.e., the slope of the Arrhenius plot. This makes the design matrix, and hence the solution, highly sensitive to inaccuracies in E_a. An additional advantage to using $\ln(D/a^2)$ values rather than a regressed function $D(T)/a^2$ is the complete lack of dependence upon the temperature of each step. This may be particularly advantageous if working with phases (e.g., garnet) that require extraction temperatures unattainable using the methods of [34] (> 600°C) and lower than those easily calibrated using optical pyrometry (< 1000°C). Extraction steps in this temperature range could be used for a profile inversion even if not used to determine $D(T)/a^2$. However, direct use of $\ln(D/a^2)$ values eliminates the statistical advantage of determining diffusion coefficients by least squares regression.

To minimize the propagation of analytical un-

certainties into the resulting profile each of the inversions was regularized according to its analytical error [4] by identifying a characteristic break in slope in a plot of $|u_i^T \mathbf{f}|$ vs. singular value index i (see fig. 4c in [4] as an example). In these inversions, the indices at which errors dominated the solution were easily recognized.

The three inversions are presented in Fig. 4. Note that the ordinate extends from 0.5 to 1.0, and that all curves converge to $C/C(0) = 1.0$ for values of $r/a < 0.5$. We used D/a^2 values calculated for each step. We find good agreement between the shapes of each inversion and the predicted profiles. We also find good agreement in the integrated gas contents. By comparison with the expected profiles, the inversions in Fig. 4 roughly indicate the uncertainties expected for profiles derived by this approach. The inverse calculations estimate the shape of each ^{4}He distribution and deficit gas fraction reasonably well. The worst match (the 6% deficit gas fraction inversion) was off by only $\sim 0.5\%$ (0.055 vs. 0.060). The

Fig. 4. Radial concentration profiles. Shown are the ^{4}He concentration C (normalized to the concentration at the center of the domain, $C(0)$) at the radial position r (normalized to domain radius, a) within the spherical domain. Solid lines were calculated by inverting Durango apatite data using [4] and as discussed in the text. Dashed lines are the predicted profiles based on isothermal outgassing assuming initially uniform ^{4}He and spherical geometry. The numbers indicate deficit gas fractions calculated by integrating the profiles.

other two profiles agree in deficit gas fraction extremely well. We did observe a systematic 'overshoot' in each of the profiles with $C/C(0)$ values slightly larger than 1.0 for $r/a \approx 0.8$; it is unclear if this is a general artifact associated with the calculation. Note that because the Durango apatite contains a discontinuous ^{4}He concentration profile at $r/a = 1.0$, we do not include the 0% deficit gas fraction inversion [4].

5.6. The spherical model

The representation of a He distribution within a spherical diffusion domain is an analytically tractable model that clearly does not apply perfectly in nature. An important question for our technique is how this imperfect assumption affects the results. Using stepwise release data for a uniformly distributed gas (^{3}He), the formulation of [10] produces diffusivities D/a^2 corresponding to a model spherical domain of radius a with a surface area to volume ratio approximating that of the actual domain. This model yields self-consistent results even when non-spherical geometries are used, provided He diffusion is crystallographically isotropic. The latter has been shown to be true in the case of apatite [16], but has not been established for other minerals.

In the case of Durango apatite, grains are angular shards, not spheres [16], so the Durango experiment provides a good test of this supposition. The He distribution within the shards following diffusive loss will be a complicated function controlled by three-dimensional shard geometry. For instance thin slab-like features with locally high surface to volume ratio should be stripped of He more efficiently than spherical features. Nevertheless, the Fechtig and Kalbitzer [10] calculation produces $\ln(D/a^2)$ values that are linear when plotted vs. $1/T$ and can be used to describe the ^{4}He distribution following diffusive loss. The calculation effectively averages over the geometrically complicated nature of the material and returns a diffusion domain radius, a (i.e., $\ln(D/a^2)$), which on the average describes the characteristic diffusion length scale of the material.

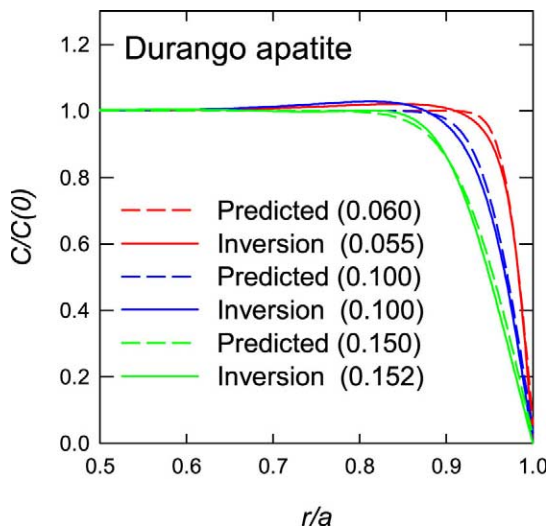Figs. 2a and 4 illustrate the self-consistency of

this example. Using the calculated $\ln(D/a^2)$ values, the inversions recover the expected profiles after diffusive rounding despite the fact that these profiles *cannot* be simple radially symmetric spheres. This is a significant result in that it indicates that the spherical model can be used to describe a natural ^{4}He distribution. As we showed previously [4], as long as the domain geometry and diffusion coefficients are self-consistently applied, the profiles obtained by inversion or forward model matching can be used to constrain a sample's low-temperature cooling trajectory in nature even if the sample is not spherical.

5.7. Original domain surfaces

Unlike a standard He diffusion experiment [9,16,17], it is critically important that a He profiling experiment be performed on diffusion domain(s) with original, intact surfaces. Most of the t–T information contained within a concentration profile is located toward the domain's outer edge [4]. If individual crystals or grains define the diffusion domain(s) of a sample, broken fragments and/or missing surfaces would result in incorrect results. In samples with a naturally rounded distribution, broken surfaces would cause erroneously elevated ^{4}He release in the initial steps of an experiment and would invert to a more square profile than actually exists.

5.8. Future directions

Given the spallation ^{3}He yields listed in Table 1, we can produce a high-quality ratio evolution diagram from as little as ∼250 μg of irradiated material. However, single crystals of relevant minerals, e.g., apatite, titanite and zircon, typically weigh just a few μg; at present we must analyze crystal aggregates. Proton-induced ^{3}He production drops off at energies below ∼30 MeV, and only modestly increases above 150 MeV [5], so changing the energy of the protons will not yield much more ^{3}He. Increasing the proton fluence through longer or more intense irradiation is the obvious way to increase ^{3}He yield. Based on the ^{3}He yields and the detection limit in our laboratory, a 10-fold increase in fluence should permit single-crystal experiments. This ability should permit new applications for He isotope geochemistry [4].

6. Conclusions

We have shown that a uniform ^{3}He distribution can be artificially produced within minerals by irradiation with a 150 MeV proton beam. We demonstrated that the outgassing of spallation ^{3}He can be used as a proxy for radiogenic ^{4}He diffusion. Proton-induced ^{3}He can therefore be used for determining natural He distributions and for the applications described by Shuster and Farley [4]. We demonstrated that the concentration profile inversion technique [4] successfully recovers relatively simple profiles using release fractions containing typical measurement errors. The highly desirable ability to perform single-crystal analyses will require at least a 10-fold increase in the artificial ^{3}He abundance, which should be attainable.

Acknowledgements

References

[1] K.A. Farley, (U–Th)/He dating: Techniques, calibrations, and applications, in: D. Porcelli, C.J. Ballentine, R. Wieler (Eds.), Reviews in Mineralogy and Geochemistry: Noble Gases in Geochemistry and Cosmochemistry, 2002, pp. 819–844.

[2] S. Niedermann, Cosmic-ray-produced noble gases in terrestrial rocks: Dating tools for surface processes, in: D. Porcelli, C.J. Ballentine, R. Wieler (Eds.), Reviews in Mineralogy and Geochemistry: Noble Gases in Geochemistry and Cosmochemistry, 2002, pp. 731–777.

[3] R. Wieler, Cosmic-ray-produced noble gases in meteorites, in: D. Porcelli, C.J. Ballentine, R. Wieler (Eds.), Re-

views in Mineralogy and Geochemistry: Noble Gases in Geochemistry and Cosmochemistry, 2002, pp. 125–163.

[4] D.L. Shuster, K.A. Farley, ^{4}He/^{3}He thermochronometry, Earth Planet. Sci. Lett. 217 (2004) 1–14.

[5] I. Leya et al., Cross sections for the proton-induced production of He and Ne isotopes from magnesium, aluminum, and silicon, Nuclear Instrum. Methods Phys. Res. B 145 (1998) 449–458.

[6] G. Friedlander et al., Nuclear and Radiochemistry, 3rd edn., Wiley, New York, 1981, 684 pp.

[7] K.A. Farley, R.A. Wolf, L.T. Silver, The effects of long alpha-stopping distances on (U–Th)/He ages, Geochim. Cosmochim. Acta 60 (1996) 4223–4229.

[8] D. Lal, In situ-produced cosmogenic isotopes in terrestrial rocks, Annu. Rev. Earth Planet. Sci. 16 (1988) 355–388.

[9] R.A. Wolf, K.A. Farley, L.T. Silver, Helium diffusion and low-temperature thermochronometry of apatite, Geochim. Cosmochim. Acta 60 (1996) 4231–4240.

[10] H. Fechtig, S. Kalbitzer, The diffusion of argon in potassium bearing solids, in: O.A. Schaeffer, J. Zahringer (Eds.), Potassium-Argon Dating, Heidelberg, Springer, 1966, pp. 68–106.

[11] J.M. Sisterson, Personal communication; unpublished data, 2003.

[12] I. McDougall, T.M. Harrison, Geochronology and Thermochronology by the ^{40}Ar/^{39}Ar Method, 2nd edn., Oxford Monographs on Geology and Geophysics, 1999, 269 pp.

[13] O. Lovera, F. Richter, T. Harrison, The ^{40}Ar/^{39}Ar thermochronometry for slowly cooled samples having a distribution of diffusion domain sizes, J. Geophys. Res. 94 (1989) 17917–17935.

[14] K.A. Farley, P.W. Reiners, V. Nenow, An apparatus for high-precision helium diffusion measurements from minerals, Anal. Chem. 71 (1999) 2059–2061.

[15] D.B. Patterson, K.A. Farley, Extraterrestrial ^{3}He in seafloor sediments: Evidence for correlated 100 kyr periodicity in the accretion rate of interplanetary dust, orbital parameters, and quaternary climate, Geochim. Cosmochim. Acta 62 (1998) 3669–3682.

[16] K.A. Farley, Helium diffusion from apatite: general behavior as illustrated by Durango fluorapatite, J. Geophys. Res. 105 (2000) 2903–2914.

[17] P.W. Reiners, K.A. Farley, Helium diffusion and (U–Th)/He thermochronometry of titanite, Geochim. Cosmochim. Acta 63 (1999) 3845–3859.

[18] E.J. Young et al., Mineralogy and geochemistry of fluorapatite from Cerro de Mercado, Durango, Mexico, US Geol. Surv. Prof. Pap. 650 (1969) D84–D93.

[19] P.K. Zeitler et al., U–Th–He dating of apatite: a potential thermochronometer, Geochim. Cosmochim. Acta 51 (1987) 2865–2868.

[20] J. Boyce, K. Hodges, Chemical variations in the Cerro de Mercado (Durango, Mexico) fluorapatite: Assessing the effect of heterogeneity on a geochronologic standard, Eos Trans. AGU 82 (Fall Meet. Suppl.) (2001) Abstract V22C-1061.

[21] P.R. Renne et al., Intercalibration of standards, absolute ages and uncertainties in Ar-40/Ar-39 dating, Chem. Geol. 145 (1998) 117–152.

[22] M.D. Schmitz, S.A. Bowring, U–Pb zircon and titanite systematics of the Fish Canyon Tuff: an assessment of high-precision U–Pb geochronology and its application to young volcanic rocks, Geochim. Cosmochim. Acta 65 (2001) 2571–2587.

[23] R. Batiza, Petrology and chemistry of Guadalupe Island: an alkalic seamount on a fossil ridge crest, Geology 5 (1977) 760–764.

[24] K.A. Farley, A.R. Basu, K. Nilsson, Geochemistry and isotopic composition of Guadalupe Island lavas and ultramafic xenoliths, EOS Trans. AGU 72 (1991) 500.

[25] T.W. Trull, M.D. Kurz, W.J. Jenkins, Diffusion of cosmogenic ^{3}He in olivine and quartz: implications for surface exposure dating, Earth Planet. Sci. Lett. 103 (1991) 241–256.

[26] T.W. Trull, M.D. Kurz, Experimental measurements of ^{3}He and ^{4}He mobility in olivine and clinopyroxene at magmatic temperatures, Geochim. Cosmochim. Acta 57 (1993) 1313–1324.

[27] T.W. Trull, M.D. Kurz, Isotopic fractionation accompanying helium diffusion in basaltic glass, J. Mol. Struct. 485 (1999) 555–567.

[28] L.C. Luther, W.J. Moore, Diffusion of helium in silicon germanium+diamond, J. Chem. Phys. 41 (1964) 1018.

[29] P.etal. Horn, ^{39}Ar-^{40}Ar dating of lunar rocks: Effects of grain size and neutron irradiation, Geochim. Cosmochim. Acta 6 (Suppl. Proceedings of Sixth Lunar Science Conference) (1975) 1563–1591.

[30] R.C. Wiens et al., Helium isotope diffusion in natural diamonds, Geochim. Cosmochim. Acta 58 (1994) 1747–1757.

[31] T.C. Onstott et al., Recoil refinements – Implications for the Ar-40/Ar-39 dating technique, Geochim. Cosmochim. Acta 59 (1995) 1821–1834.

[32] L.T. Chadderton, Radiation Damage in Crystals, Wiley, New York, 1965, 202 pp.

[33] D. Shuster, K.A. Farley, P. Vasconcelos, Geochronology of weathering processes by (U–Th)/He analysis of supergene goethite and cryptomelane, EOS Abstr. 81 (2001) 1263.

[34] K. Farley, P. Reiners, V. Nenow, An apparatus for high-precision helium diffusion measurements from minerals, Anal. Chem. 71 (1999) 2059–2061.